Journal of the Physical Society of Japan
Vol. 76, No. 11, November, 2007, 114201

Multilayer Scintillator Responses for Mo Observatory of Neutrino Experiment Studied Using a Prototype Detector MOON-1

Hidehito NAKAMURA[1*], Peter J. DOE[2], Hiroyasu EJIRI[1,2,3], Steven R. ELLIOTT[2,4], Jonathan ENGEL[5], Miroslav FINGER[6], Michael FINGER, Jr.[6], Kenichi FUSHIMI[7], Victor M. GEHMAN[2,4], Mark B. GREENFIELD[8], Vo H. HAI[9], Ryuta HAZAMA[10], Hitoshi IMASEKI[1], Petr KAVITOV[11], Vladimir D. KEKELIDZE[12], Hisashi KITAMURA[1], Kenji MATSUOKA[9], Masaharu NOMACHI[9], Takeo OGAMA[9], Adam PARA[13], R. G. Hamish ROBERTSON[2], Takuya SAKIUCHI[9], Tatsushi SHIMA[3], Milos SLUNECKA[6], Grigori D. SHIRKOV[12], Alexei N. SISSAKIAN[12], Alexander I. TITOV[12], Yukio UCHIHORI[1], Saori UMEHARA[9], Atsushi URANO[9], Vladimir VATURIN[11], Victor V. VORONOV[12], John F. WILKERSON[2], Douglas I. WILL[2], Kensuke YASUDA[7], and Sei YOSHIDA[14]

[1]*NIRS, National Institute of Radiological Sciences, Chiba 263-8555*
[2]*CENPA, University Washington, Seattle, WA 98195, USA*
[3]*RCNP, Osaka University, Ibaraki, Osaka 567-0047*
[4]*LANL, P.O.Box 1663, MSH 803, Las Alamos, NM 87545, USA*
[5]*Physics and Astronomy, University of North Carolina, Chapel Hill, NC 27599, USA*
[6]*Charles University, FMP, CZ-18000 Praha 8, Czech Republic*
[7]*IAS, University of Tokushima, Tokushima 770-8592*
[8]*Physics, International Christian University, Tokyo 181-8585*
[9]*OULNS, Physics, Osaka University, Toyonaka, Osaka 560-0043*
[10]*Hiroshima University, Higashi Hiroshima, Hiroshima 739-8527*
[11]*VNIIEF, 607188, Sarov, Nizhny Novgorod Region, Mira Ave, 37, Russia*
[12]*Joint Institute for Nuclear Research, 141980 Dubna, Russia*
[13]*FNAL, P.O.Box, 500, Batavia, IL 60510-0500, USA*
[14]*RCNS, Tohoku University, Sendai 980-8578*

(Received June 19, 2007; accepted August 16, 2007; published October 25, 2007)

An ensemble of multilayer scintillators is discussed as an option of the high-sensitivity detector MOON (Mo Observatory of Neutrinos) for spectroscopic measurements of neutrinoless double beta decays. A prototype detector MOON-1, which consists of 6-layer plastic scintillator plates, was built to study the photon responses of the MOON-type detector. The photon responses, i.e., the number of scintillation photons collected and the energy resolution, which are key elements for high-sensitivity experiments, are found to be 1835 ± 30 photoelectrons for 976 keV electrons and $\sigma = 2.9 \pm 0.1\%$ ($\Delta E/E = 6.8 \pm 0.3\%$ in FWHM) at the $Q_{\beta\beta} \sim 3$ MeV region, respectively. The multilayer plastic scintillator structure with high energy resolution as well as a good signal for the background suppression of β–γ rays is crucial for the MOON-type detector to achieve inverted-hierarchy neutrino-mass sensitivity. It will also be useful for medical and other rare-decay experiments as well.

KEYWORDS: neutrino mass, double beta decay, plastic scintillator, energy resolution
DOI: 10.1143/JPSJ.76.114201

1. Introduction

Double beta decays (DBD) are sensitive and realistic probes for studying the Majorana nature of neutrinos (ν) and the absolute ν-mass spectrum. The effective neutrino mass to be studied by DBD is of the order of 100 or 20 meV, in case of the quasi-degenerate (QD) or the inverted-hierarchy (IH) mass spectrum respectively. It is much smaller in the case of the normal hierarchy (NH). In fact, the effective mass also depends on the Majorana phases.

Current $0\nu\beta\beta$ experiments are limited by mass sensitivity of the order of 300 meV because of the limited total number of $\beta\beta$ isotopes. Several experiments are planned for the study of the effective mass in the QD and IH mass regions. Detailed discussions on ν-masses studied by DBD and future DBD experiments can be found in review articles and the references therein.[1–6)]

The present paper is concerned with the MOON (Mo Observatory of Neutrinos)-type spectroscopic detector,[7)] which is based on the ELEGANT V detector,[8–10)] but is expanded to improve the half-life sensitivity by orders of magnitude for studying the effective mass in the QD and IH mass regions.

Spectroscopic (tracking) experiments such as MOON[7)] and NEMO[11,12)] are complementary to the calorimetric experiments of Majorana/GERDA,[13,14)] CUORE,[15,16)] EXO,[17)] COBRA,[18)] and others. Since $\beta\beta$ sources are separated from the spectroscopic detectors, $\beta\beta$ isotopes with large $Q_{\beta\beta}$ values are selected to archive high mass sensitivity. Then, the energies of $0\nu\beta\beta$ signals exceed those of most β signals from U–Th chain isotopes, ^{60}Co, ^{40}K, and other radioactive isotope (RI) impurities. Thus their background (BG) rates are not critical. Major BG events are due to the tail of the $2\nu\beta\beta$ spectrum in the $0\nu\beta\beta$ window, which depends strongly on the $0\nu\beta\beta$ energy window and thus on the energy resolution.

The key points of spectroscopic experiments on the QD-IH masses are to build a large low-background detector to accommodate $\beta\beta$ isotopes of the order of $n_{\beta\beta} \approx 1$ (ton) and to achieve sufficient energy resolution with $\sigma \approx 2.2$–3% ($\Delta E/E \approx 5$–7% in FWHM) in the $Q_{\beta\beta}$ value region.[1,7,19)]

*E-mail: hidehito@nirs.gojp

MOON aims at a half-life sensitivity of approximately $(2.5-6) \times 10^{26}$ y, which corresponds to the QD-IH mass sensitivity of 52–32 meV with the nuclear matrix element of $M = 3$. The uncertainty of around $\pm 50\%$ in M leads to the similar uncertainty in the mass. The solid-scintillator facility of MOON consists of multilayer detector modules.[7,20–23] Each module is composed of a plastic scintillator plate, two thin detector planes for positioning and particle identifying, and a thin $\beta\beta$ source film interleaved between the two planes.

The position of the $\beta\beta$ vertex point is identified using the detector planes, while the energies of the two β rays are measured by two adjacent plastic scintillator plates. All other modules (layers) are used as active shields to reject γ rays and neutrons. Scintillation photons are collected by photo multiplier tubes (PMTs) around the plastic scintillator plate.

In the case that each module is composed of one plastic scintillator of dimensions $\sim 1 \times 1 \times 0.015\,\mathrm{m}^3$ and a thin $\beta\beta$ source film of size $100 \times 100\,\mathrm{cm}^2$ and thickness $20\,\mathrm{mg/cm}^2$, the detector contains 0.2 kg of $\beta\beta$ isotopes per module. Thus, one unit made of 100 modules contains 30 kg of $\beta\beta$ isotopes with a total detector volume of the order of $\sim 1 \times 1 \times 5\,\mathrm{m}^3$ in the case of MWPC planes used for particle identification. The MOON-type spectroscopic experiment has several unique features.

(1) Individual β rays from $0\nu\beta\beta$, which are emitted in opposite directions, are measured in coincidence using two adjacent plastic scintillator plates to confirm the ν-mass term in the $0\nu\beta\beta$.
(2) The multimodule structure makes it feasible to build a compact detector with $\sim 0.2\,\mathrm{m}^3$ per kg of $\beta\beta$ isotopes to accommodate ton-scale $\beta\beta$ isotopes.
(3) High energy resolution of $\sigma \approx 2.2-3\%$ at $Q_{\beta\beta}$ values of ~ 3 MeV may be obtained by efficient photon collection to reduce the $2\nu\beta\beta$ contribution.
(4) The multilayer module structure with a good position resolution may enable one to select $0\nu\beta\beta$ signals and reject RI background signals.[1,7,20,21] Actually, a Monte Carlo simulation[19] for U–Th impurities of 20 m Bq/t gives a BG rate of the order of 0.1/t y at the $0\nu\beta\beta$ window after space-correlation and time-correlation cuts.
(5) Since the source is separated from the detector, one can select $\beta\beta$ nuclides from the viewpoints of the nuclear matrix element, the phase space, the signal energy, and the $2\nu\beta\beta$ rate.

The present paper aims at demonstrating the experimental feasibility of constructing a multilayer scintillator system to study the photon response with the high energy resolution using a prototype MOON-1 detector.[21–27]

The prototype MOON-1 detector was built to study the ν-mass sensitivity of the MOON-type detector. In the present report, we mainly discuss the photon responses, i.e., the scintillation photon collection, the energy resolution, and the energy calibration, which are important for high-sensitivity experiments. The prototype MOON-1 detector is described in §2. The scintillation photon collection, the energy resolution and the energy calibration are discussed in detail in §3. Concluding remarks are given in §4.

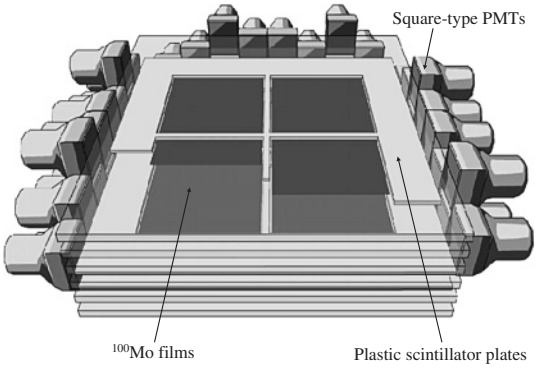

Fig. 1. Schematic view of the MOON-1 detector with 6-layer plastic scintillator plates and 11 ^{100}Mo foils. The ^{100}Mo foils are interleaved between two plastic scintillator plates. The total mass of ^{100}Mo is 142 g. The plastic scintillator plates are viewed using square-type PMTs (R6236-01-KMOD provided by Hamamatsu Photonics). The 56 PMTs are coupled to the four sides of the 6 plastic scintillator plates.

2. Prototype MOON-1 Detector

2.1 *MOON-1 detector configuration*

The prototype MOON-1 detector was constructed to study the scintillation photon responses (photon collection and energy resolution), the feasibility of multilayer structures of plastic scintillator plates and $\beta\beta$-source films, and the BG-rejection capability. These are crucial points for high-sensitivity experiments, and thus the results of MOON-1 can be used to prove the feasibility of MOON with IH mass sensitivity of the order of 30–50 meV.

The MOON-1 detector consists of 6-layer plastic scintillator plates, each of $53 \times 53 \times 1\,\mathrm{cm}^3$, as shown schematically in Fig. 1.[26,27] RP-408 (BC-408 equivalent) plastic scintillator plates were provided by REXON. The plastic scintillator plates are realistic detectors from the view points of low RI impurities, a good photon yield of around 10^4 per MeV, and the low cost of a large quantity on the order of 10 tons, as used in refs. 8 and 28. In fact, β–γ BG from ^{214}Bi in the plastic scintillator, which exceeds the $0\nu\beta\beta$ signal in energy, is vetoed by measuring the post-α decay in the same plastic scintillator.

The 94.5% enriched ^{100}Mo foils,[29] each having dimensions of $18 \times 18\,\mathrm{cm}^2$ and a thickness of $40\,\mathrm{mg/cm}^2$, are interleaved between plastic scintillator plates in the MOON-1 detector. The ^{100}Mo foils are covered with aluminized Mylar films having surface areas of $53 \times 53\,\mathrm{cm}^2$ and a thickness of $6\,\mu\mathrm{g/cm}^2$. The aluminized Mylar films suppress the photon crosstalk between the adjacent plastic scintillator plates and support the ^{100}Mo foils.

The six-layer plastic scintillator plates are viewed using $6 \times 6\,\mathrm{cm}^2$ square-type PMTs R6236-01-KMOD provided by Hamamatsu Photonics. The PMTs have a K-free window with 0.7 Bq ^{40}K. The 56 PMTs are coupled to the four sides of the 6-layer plastic scintillator plates. Side-surface coverage of the plastic scintillator plates by the PMT photosensitive areas is about 82% excluding the dead space of each PMT surface. A silicone cookie, which is made from a silicone rubber SE1821 provided by TORAY, is used as an optical connection with ≈ 3 mm in thickness. Each PMT collects photons from three plastic scintillator plates, and the hit plastic scintillator plate is identified by the PMT hit pattern.

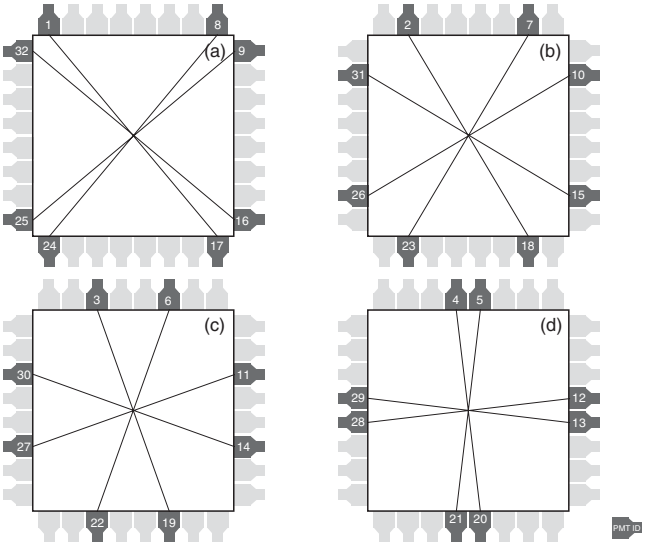

Fig. 2. PMT geometry. (a)–(d) show four kinds of PMT geometrical positions. Eight PMTs in the each geometry are symmetrical with respect to the test source at the center. PMT ID numbers are shown for PMTs.

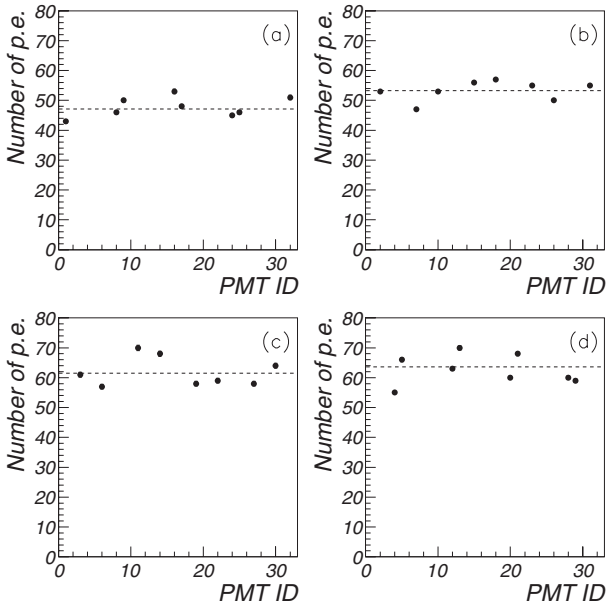

Fig. 3. Number of photoelectrons obtained by each PMT. ^{207}Bi source with 976 keV K conversion electrons is set at the center of the plastic scintillator.

2.2 *Photon response of plastic scintillator*

The photon response for the same plastic scintillator as that used for the MOON-1 detector was studied using RI sources. Thirty-two PMTs are coupled to the four sides of the plastic scintillator to give the same coverage as that in the MOON-1 detector. As the first step, the photon response for the PMT was measured using photons from a light emitting diode (LED; NSPB500S, 475 nm) provided by NICHIA. The measured spectrum was analyzed in terms of the Poisson distribution for the photoelectron fluctuation and the Gaussian distribution for the PMT gain fluctuation. The PMT response is obtained to be 3.6 ± 0.07 ADC channels per photoelectron. The error is due to statistical fluctuation obtained by fitting.

Before assembling the six-layer plastic scintillator plates in the MOON-1 detector, the photon response for each plastic scintillator plate was measured using a 976 keV K conversion electron from a ^{207}Bi source at the center of the plastic scintillator plate. The number of photoelectrons for each PMT was deduced from the observed 976 keV peak channel using the measured response of 3.6 channels per photoelectron. The number of photoelectrons depends upon the geometrical position (solid angle) of PMTs with respect to the source, as shown in Figs. 2(a)–2(d), and is plotted for the four PMT geometries in Fig. 3. The number of photoelectrons is nearly the same among PMTs in approximately the same relative geometrical position [Figs. 2(a)–2(d)]. They are slightly scattered around the average values (the dotted lines in Fig. 3), depending on the photocontact between the PMT and the plastic scintillator plate. In order to obtain the average value at each PMT, a slight adjustment was made among the 8 PMTs having the same relative geometry.

Then the energy spectrum is obtained for the K and L conversion electron lines from the ^{207}Bi source by summing the energy signals from the 32 PMTs. The obtained spectrum is shown as a function of the number of photoelectrons in Fig. 4. The total number of photoelectrons is 1830 ± 35 for

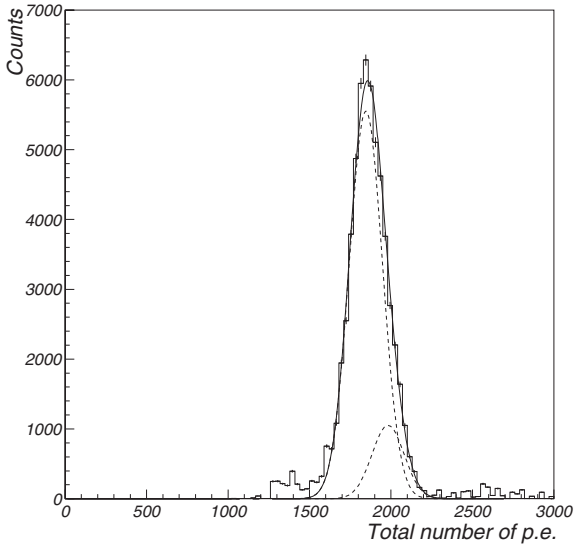

Fig. 4. Energy spectrum of the K and L conversion electrons from ^{207}Bi obtained by summing the energy signals from the 32 PMTs and fitting using the two Gaussian peaks of the K and L conversion electron lines.

the K conversion electron line (976 keV), which corresponds to 1860 photoelectrons per MeV. This is precisely the values expected from the total number of 10^4 photons per MeV for the present plastic scintillator,[30] the total reflection rate of the plastic scintillator, the amount of coverage of the four sides of the plastic scintillator by the PMTs, and the photoelectron conversion coefficient of 0.25.[31] The energy resolution of the plastic scintillator is derived by fitting the observed spectrum using two Gaussian peaks of K (976 keV) and L (1048 keV) conversion electron lines. Here the relative K- and L-peak yields are known and the energy resolution is assumed to follow a $\sigma/\sqrt{E}$ dependence. The energy resolution is found to be $\sigma = 4.8 \pm 0.2\%$ ($\Delta E/E = 11.4 \pm 0.5\%$ in FWHM) at 976 keV, as shown in Fig. 4.

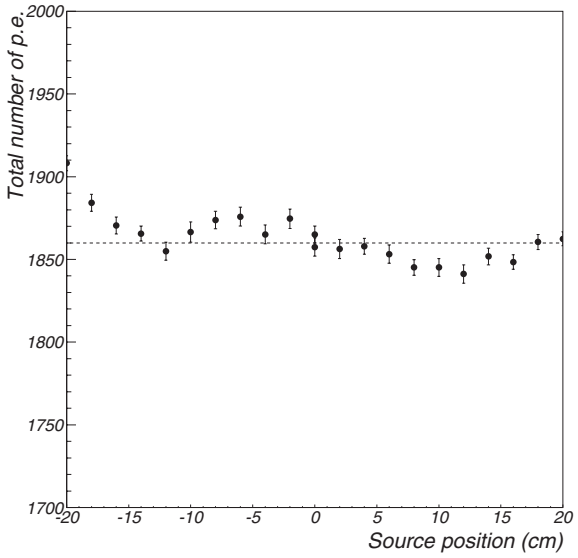

Fig. 5. Position dependence of the total number of photoelectrons from the 976 keV ^{207}Bi K-line. The source position is given by the distance along the x axis $(x, y = 0)$ from the center $(x, y) = (0, 0)$.

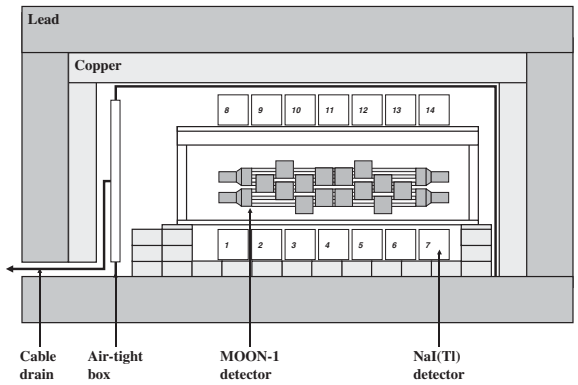

Fig. 6. Experimental setup of MOON-1 detector. The MOON-1 detector is set in the active and passive shields of ELEGANT V. Fourteen NaI(Tl) detectors are used as the active shield. These detectors are placed in an airtight box to keep the Rn concentration low. Copper and lead bricks are used as the passive shield.

The total number of photoelectrons has little dependences (a few %) on the source position, as shown in Fig. 5. Since the source position can be derived from the relative yields of the photoelectrons at the four sides, one can correct the slight position dependence.

2.3 *MOON-1 detector setting*

The MOON-1 detector was set in the active and passive shields of ELEGANT V,[8,27] as shown in Fig. 6. The drift chamber was replaced by the multilayer plastic scintillator plates with ^{100}Mo foils. An active shield consisting of 14 NaI(Tl) detectors, each having dimensions of $102 \times 10.2 \times 10.2\,\mathrm{cm}^3$, was used to veto γ rays associated with RI backgrounds. The passive shield consists of 10-cm-thick copper bricks (oxygen free high conductivity) and 15-cm-thick lead bricks. The MOON-1 and the NaI(Tl) detectors were set in an airtight box (69.6 cm high and $147.0\,\mathrm{cm} \times 200.0\,\mathrm{cm}^2$) in order to keep the radon (Rn) concentration low by flushing it with Rn-free N_2 gas. The experiment was carried out at the Oto underground laboratory at a 1400 m water-equivalent depth.

Data are collected using four kinds of trigger signals: from the plastic scintillators, LED, clock, and NaI(Tl) detector. The first three triggers were generated simultaneously. The plastic scintillator trigger, with a threshold of less than 200 keV, is used to measure the two β rays by plastic scintillators. The LED trigger is used to monitor the MOON-1 detector. The clock trigger is used to obtain the pedestal for each PMT. The NaI(Tl) trigger is used to measure the γ ray background. The data are recorded using ORed triggers. The ORed rate for the background measurement is around 11 Hz, with 8, 2, and 1 Hz arising from the plastic scintillators, LED, and clock, respectively. The dead time is 1.2 ms (∼1%).

The front end of the acquisition system is designed using CAMAC at the Oto underground laboratory. The CC/NET (TOYO),[32] which contains a CPU, is used as the CAMAC crate controller. A Linux OS is installed in the CC/NET, the collected-data program runs on the Linux OS. The data, which are saved in the server computer, are transferred to the computer at the Research Centre for Nuclear Physics (RCNP) of Osaka University and its quality is checked via the network.

High voltage (HV) is supplied from CAEN SY 527[33] and SY 403[34] for the PMTs in the MOON-1 plastic scintillators and the NaI(Tl) detector, respectively. They can be controlled and monitored by the Linux server through RS232C. Therefore, we can access the Oto underground laboratory from outside.

3. MOON-1 Detector Responses

3.1 *Beta event selection*

The present results demonstrate the feasibility of the multilayer plastic scintillator modules in terms of having both sufficient scale and energy resolution, which are key elements for such a high-sensitivity experiment. Here, single-layer hit events at PL3 (the third layer from the top) are selected to estimate the energy resolution of the MOON-1 plastic scintillator plates.

The experimental setup is shown in Fig. 7. Photoresponses were studied by using 1.274 MeV γ rays from a ^{22}Na source, which was set 90 mm above the top of the plastic scintillator plate. One PMT collects photons from 2 or 3 plastic scintillator layers. The selection of the single-layer PL3 event is made by requesting signals from PMTs viewing PL3 and no (veto) signals from other PMTs, as shown schematically in Fig. 8. The energy deposited on PL3 is obtained by summing the signals from PMTs viewing PL3. Here the threshold for the summed signal is set at 200 keV, while that for the veto signal is 50 keV.

3.2 *Gamma ray reconstruction and energy calibration*

Compton scattering is a dominant process for γ rays in the plastic scintillator. Then the full-energy γ peak can be reconstructed by summing the energy of the Compton scattered electron at one plastic scintillator and the energy of the Compton scattered γ ray at one NaI(Tl) detector. The single-layer hits at PL3 and the energy deposits at NaI-ID4 are required for the 1.274 MeV γ rays from the ^{22}Na source, as shown in Fig. 9. The other NaI(Tl) detectors are used as

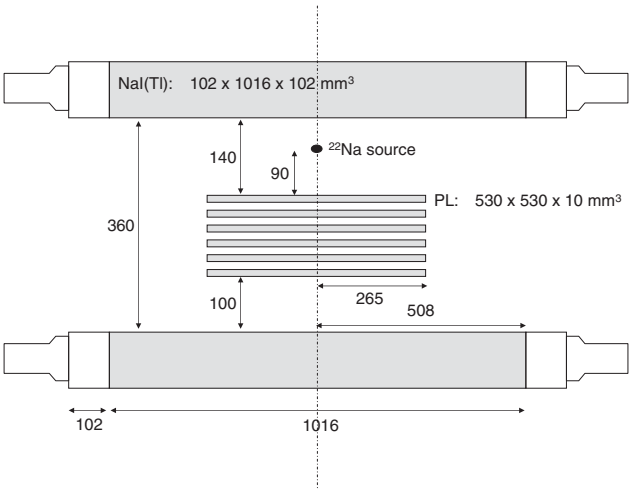

Fig. 7. Experimental setup for the energy calibration. A ^{22}Na source is set 90 mm above the top of the plastic scintillator.

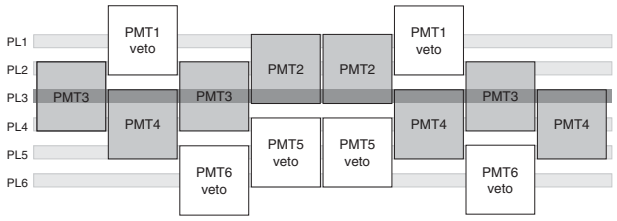

Fig. 8. Plastic scintillator and PMT configuration. Single-layer hit events are selected by requesting signals from PMT2, PMT3, and PMT4 in coincidence and no (veto) signals from PMT1, PMT5, or PMT6.

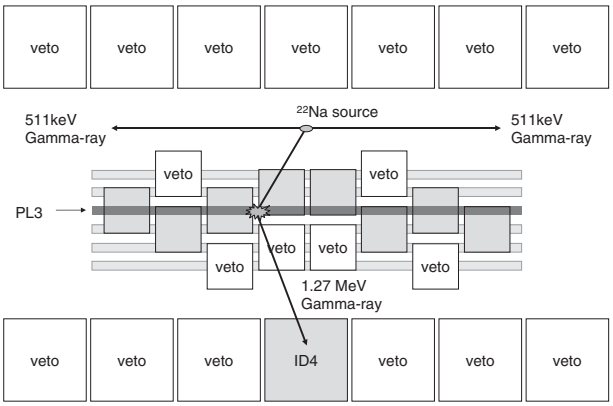

Fig. 9. Compton scattering of ^{22}Na γ rays. The γ ray source is set roughly at the center of the plastic scintillator. The single-layer hit events of the plastic scintillator (PL3) followed by the signals from the NaI(Tl) detector (ID4) are selected for the 1.274 MeV γ rays from the ^{22}Na source.

veto counters. Therefore, the two 511 keV γ rays from the ^{22}Na source are emitted outside the MOON-1 detector.

The energy correlation between PL3 and NaI-ID4 is shown in Fig. 10. The line indicates the full energy of the original 1.274 MeV γ rays before Compton scattering. The reconstructed 1.274 MeV γ ray spectrum is obtained by summing the two signals from PL3 and NaI-ID4, as shown in Fig. 11.

The energy calibration is divided into two procedures. One is relative calibration. The other one is absolute energy

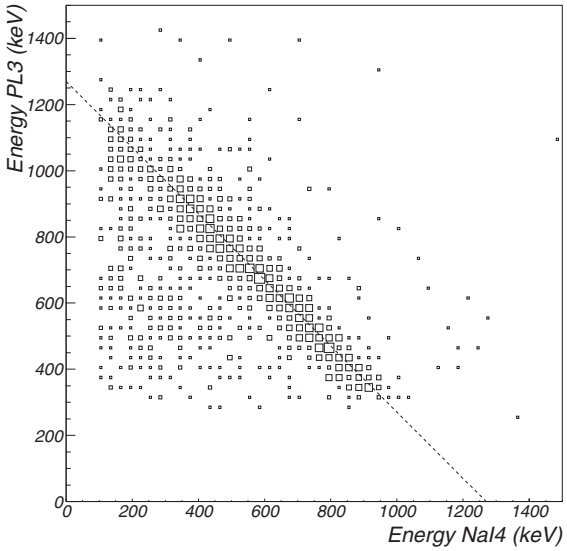

Fig. 10. Energy deposits on the plastic scintillator (PL3) and the NaI(Tl) ID4 detector shown for the 1.274 MeV γ rays from the ^{22}Na source. The line shows the sum of the energy deposits on the PL and NaI(Tl) detectors.

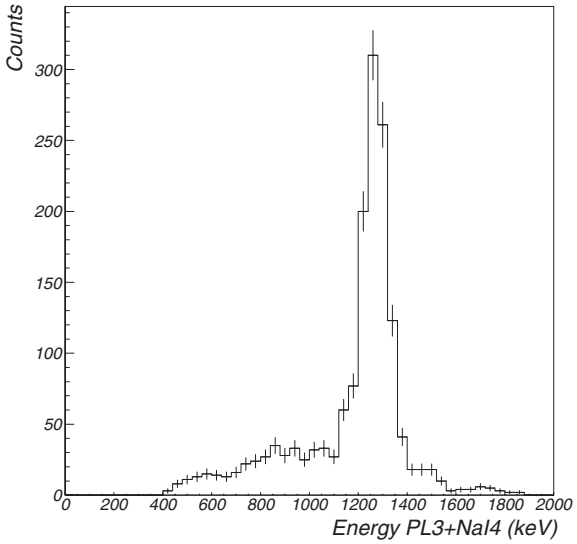

Fig. 11. Single-layer hit events from the plastic scintillator (PL3). The full energy peak of this γ ray is obtained by summing the energy deposits on the plastic scintillator (PL3) and the NaI(Tl) detector (ID4).

calibration. The relative gains of all PMTs are calibrated by using the γ rays (^{22}Na, 1.274 MeV), as shown in Fig. 9. Here the Compton scattered electron signals from the plastic scintillator are used. They have the measured distribution obtained in §2.2. The absolute energy calibration of NaI-ID4 is performed using γ rays from the source (^{22}Na 511 keV, 1.274 MeV) and natural radioactive isotopes (^{40}K 1.460 MeV, ^{208}Tl 2.615 MeV). The reconstructed peak is used for the absolute energy calibration of the plastic scintillator. This method is also used for the other plastic scintillator layers.

3.3 Energy resolution of plastic scintillator

A new method of evaluating the plastic scintillator response for low-energy electrons is carried out using reconstructed γ peaks from the Compton scattered electrons

Table I. Energy resolution of the plastic scintillator for various energy regions.

Energy[a] E_Σ (keV)	Resolution[b] σ_Σ (keV)	Energy[a] E_{NaI} (keV)	Resolution σ_{NaI} (keV)	Energy[a] E_{PL} (keV)	Resolution σ_{PL} (keV)
1274 (^{22}Na)	48.8 ± 2.4	511	22.8 ± 0.9	763	43.1 ± 2.6
1460 (^{40}K)	55.7 ± 3.0	511	22.8 ± 0.9	949	50.8 ± 3.1
2615 (^{208}Tl)	72.8 ± 9.2	1274	35.7 ± 0.8	1341	62.1 ± 9.1
2615 (^{208}Tl)	71.7 ± 8.1	800	28.2 ± 0.8	1815	67.1 ± 8.1
2615 (^{208}Tl)	74.1 ± 12.1	511	22.8 ± 0.9	2104	70.5 ± 2.2

a) E_Σ, E_{NaI}, and E_{PL} are the energy of the reconstructed γ rays, the energy deposited on the NaI(Tl) detector, the energy deposited on the plastic scintillator, respectively.

b) σ_Σ is the energy resolution for the reconstructed γ rays when the energy window of the NaI(Tl) detector is set at the energy E_{NaI}.

at the plastic scintillator and the Compton scattered γ rays at the NaI(Tl) detector. Here, the energy and the energy resolution for the reconstructed γ rays are expressed as

$$E_\Sigma = E_{PL} + E_{NaI} \quad (1)$$

$$\Delta E_\Sigma^2 = \Delta E_{PL}^2 + \Delta E_{NaI}^2, \quad (2)$$

where E_Σ, E_{PL}, and E_{NaI} are the energy of the reconstructed γ rays, the energy deposited on the plastic scintillator, and the energy deposited on the NaI(Tl) detector, respectively, and ΔE_Σ, ΔE_{PL}, and ΔE_{NaI} are their respective fluctuations.

First, the energy resolutions of the NaI(Tl) detector were found to be $\sigma_{NaI} = 4.5 \pm 0.2\%$ and $2.8 \pm 0.1\%$ for the full-energy peaks of γ rays from the source (^{22}Na 511 keV and 1.274 MeV) and to be $\sigma_{NaI} = 2.7 \pm 0.1\%$ and $2.0 \pm 0.1\%$ for those from natural radioactive isotopes (^{40}K 1.460 MeV and ^{208}Tl 2.615 MeV), respectively. Results are shown in Table I.

The energy correlation of the Compton scattered γ rays measured by the NaI(Tl) detector and the Compton scattered electrons measured by the plastic scintillator are shown for the case of the 1.274 MeV γ rays in Fig. 12. The energy window of the NaI(Tl) detector, which was used to measure the Compton scattered γ rays from the 1.274 MeV γ ray, was set at the 511 keV region, where the energy resolution of the NaI(Tl) detector was known. Then, the energy of the Compton scattered electrons, which was measured by PL3, is $E_{PL} = E_\Sigma - E_{NaI} = 1274 - 511 = 763$ keV. The reconstructed spectrum, i.e., the sum of the NaI(Tl) detector and the plastic scintillator signals for this energy window, is shown in Fig. 13.

The reconstructed spectra for 1.460 and 2.615 MeV γ ray peaks from the natural radioactive isotopes of ^{40}K and ^{208}Tl are shown for the energy window $E_{NaI} = 511$ keV of the NaI(Tl) detector in Figs. 13–15. They reflect the NaI resolution σ_{NaI} at 511 keV and the PL resolution σ_{PL} at $1460 - 511 = 949$ keV, and the NaI resolution at 511 keV and the PL resolution at $2615 - 511 = 2104$ keV, respectively.

The reconstructed (sum) peak was fitted by a Gaussian peak with an exponential background tail. The measured energy deposit at PL3 agrees with the expected value of $E_{PL} = E_\Sigma - E_{NaI}$, as shown in Fig. 16. Here the energy scale of the plastic scintillator is calibrated using the 1.460 MeV γ rays from the natural radioactive isotope ^{40}K.

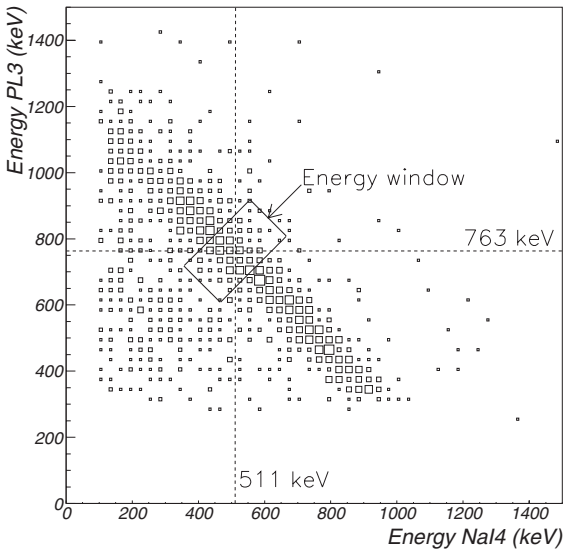

Fig. 12. Correlation between energy deposits on the plastic scintillator (PL3) and NaI(Tl) detector (ID4) for the single-layer hit events of the γ rays from ^{22}Na. The energy window of the NaI(Tl) detector is selected at the 511 keV region to estimate the energy resolution for a plastic scintillator at the $1274 - 511 = 763$ keV region. Here, the region shows the energy window. The width of the window for the 511 keV γ ray was ± 160 keV, which was $3\Delta E_{NaI}$ in the FWHM of the 511 keV peak at the NaI(Tl) detector.

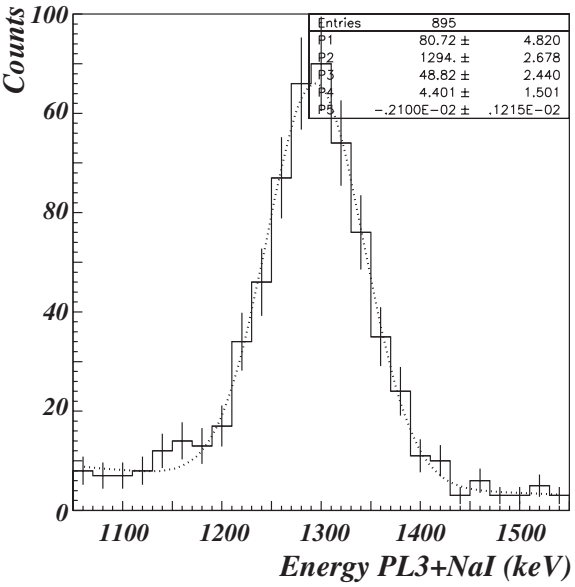

Fig. 13. Reconstructed peak of 1.274 MeV γ rays from ^{22}Na source by summing the energies of the plastic scintillator (PL3) and the NaI(Tl) detector (ID4), when the NaI(Tl) energy window is set at the 511 keV region. The dotted line is a fit using the energy resolution of $\sigma_\Sigma = 48.8 \pm 2.4$ keV at the 1.274 MeV region.

The energy resolutions of PL3 at 763, 949, and 2104 keV were obtained from the peak fits by using eq. (2) and the NaI resolution at 511 keV. Similarly, the energy resolutions of the plastic scintillator at $2615 - 800 = 1815$ keV and at $2615 - 1274 = 1341$ keV were obtained from the reconstructed spectra for the 2615 keV γ rays by selecting the energy windows at 800 and 1274 keV on the NaI(Tl) detector. They are shown in Table I.

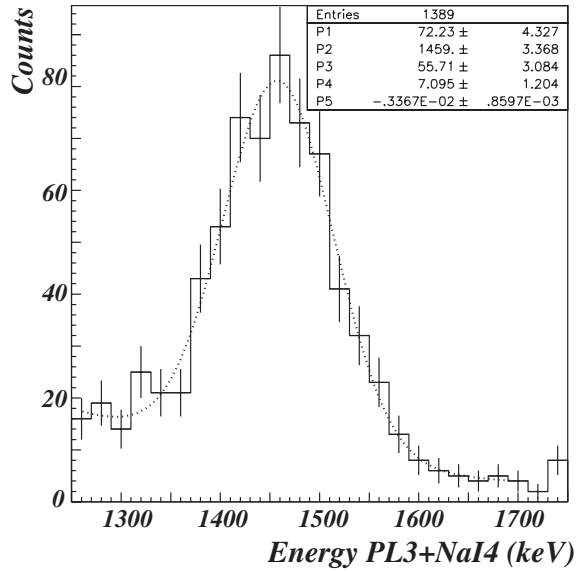

Fig. 14. Reconstructed 1.460 MeV γ peak from ^{40}K by summing the energies of the plastic scintillator (PL3) and the NaI(Tl) detector (ID4), when the NaI(Tl) energy window is set at the 511 keV region. The dotted line is a fit using the energy resolution $\sigma_\Sigma = 55.7 \pm 3.0$ keV at the 1.460 MeV region.

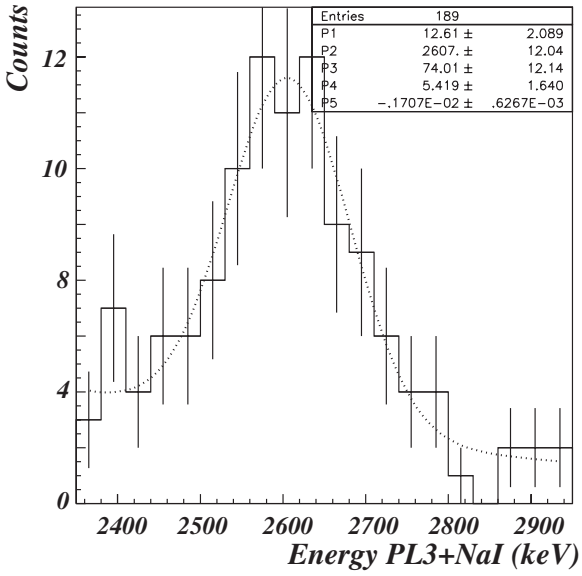

Fig. 15. Reconstructed 2.615 MeV γ peak from ^{208}Tl by summing the energies of the plastic scintillator (PL3) and the NaI(Tl) detector (ID4), when the NaI(Tl) energy window is set at the 511 keV region. The dotted line is a fit using the energy resolution $\sigma_\Sigma = 74.1 \pm 12.1$ keV at the 2.615 MeV region.

The energy resolution for PL3 is found to be well reproduced by $\sigma/\sqrt{E}$ with $\sigma = 5.0 \pm 0.2\%$ ($\Delta E/E = 11.9 \pm 0.5\%$ in FWHM) in the energy region from 0.5 to 2.1 MeV, as shown in Fig. 17 and Table I.

This energy region covers the β ray energies in most spectroscopic $\beta\beta$ experiments. The energy resolutions obtained for the conversion electrons from the source (^{137}Cs 624 keV, ^{207}Bi 976 keV) agree well with those derived from the reconstructed γ peaks, as shown in Fig. 17. The energy resolution at the ^{100}Mo $Q_{\beta\beta}$ value (3.034 MeV) is evaluated as $\sigma = 2.9 \pm 0.1\%$ ($\Delta E/E = 6.8 \pm 0.3\%$ in FWHM), which is the energy resolution required for MOON with IH mass sensitivity. The obtained energy resolution is good in view of the very large size of the plastic scintillator and the PMT coverage of only the four sides (not the top and bottom), which are important for the multilayer plastic scintillator plates in realizing a large-scale DBD detector.

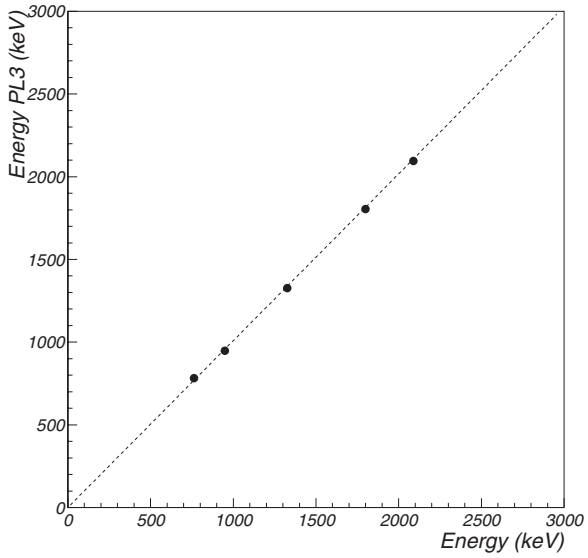

Fig. 16. Energy deposit E_{PL3} obtained from the reconstructed γ rays on the plastic scintillator PL3. The statistical error bars are within the data points.

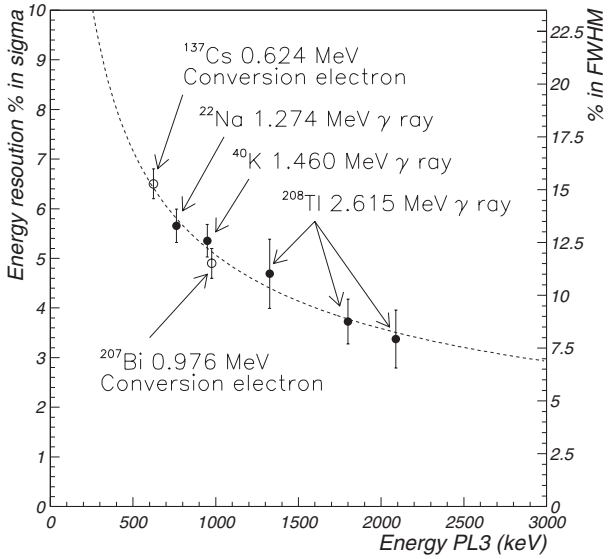

Fig. 17. Energy resolution σ and $\Delta E/E$ in FWHM of PL3 obtained from reconstructed γ rays. The x axis shows the energy deposit in PL3. The dotted line shows a fit with the energy resolution $\sigma = 5.0 \pm 0.2\%$ ($\Delta E/E = 11.9 \pm 0.5\%$ in FWHM) for 1 MeV electrons.

The present energy resolution of $\sigma = 5.0\%$ for 1 MeV electrons, however, is worse than $\sigma = 2.3\%$ due to the statistical fluctuation of the number of photoelectrons. In fact, the observed energy resolution is worse due to the nonstatistical component.[35] The nonstatistical component of the energy resolution for the plastic scintillator is found to be around $\sigma \sim 4\%$ at the 1 MeV regions.[36]

4. Concluding Remarks and Discussions

MOON is a spectroscopic $\beta\beta$ experiment with ν-mass sensitivity in the QD-IH mass region (100–30 meV).

The prototype detector MOON-1 was built to demonstrate the feasibility and photon responses of the MOON detector. It consists of 6 layers of plastic scintillator plates with dimensions of $53 \times 53 \times 1\,\mathrm{cm}^3$. Photons are collected by PMTs positioned along the four sides of the plastic scintillator plate. The energies of these multilayer plastic scintillators are shown to be well calibrated by using Compton scattered electrons from external γ sources.

The total number of photoelectrons is 1830 ± 35 for the 976 keV electron line. This is precisely the value expected for this type of plastic scintillator. The energy resolution was measured using conversion electrons from RI sources as well as Compton scattered electrons from RI γ rays. A new method of checking the plastic scintillator response for low-energy electrons was carried out using reconstructed γ peaks from the Compton scattered electrons at the plastic scintillator and the Compton scattered γ rays at the NaI(Tl) detector.

The measured energy resolution is found to be well reproduced by $\sigma/\sqrt{E}$ with $\sigma = 5.0 \pm 0.2\%$ ($\Delta E/E = 11.9 \pm 0.5\%$ in FWHM) in the energy region from 0.5 to 2.1 MeV. This leads to the energy resolution of $\sigma = 2.9 \pm 0.1\%$ ($\Delta E/E = 6.8 \pm 0.3\%$ in FWHM) at the ^{100}Mo $Q_{\beta\beta}$ value (3.034 MeV). This is precisely that required for a half-life sensitivity of 2.5×10^{26} y according to simulations[19] for MOON with 1 t of ^{100}Mo isotope. This corresponds to the QD-IH mass of around 50 meV $\pm$ 50% due to uncertainty in the $0\nu\beta\beta$ matrix element. Using ^{82}Se with a longer $2\nu\beta\beta$ half-life, a mass sensitivity of around 30 meV may be expected.

The observed energy resolution of $\sigma = 5.0\%$ for 1 MeV electrons is good in comparison with other plastic scintillator detector, but is worse than $\sigma = 2.3\%$ due to the statistical fluctuation of photoelectrons, as is well known to occur in many scintillation detectors for e-γ rays, since the observed energy resolution includes a nonstatistical component of around $\sigma \sim 4\%$.[35,36]

The reduction of the nonstatistical contribution is under progress. The photon collection efficiency depends slightly on the position of the large plastic scintillator plate, as shown in Fig. 5. It can be corrected using position-sensitive detector planes. Actually, the energy resolution is improved in the case of using a small plastic scintillator plate and by selecting the central region of the large plastic scintillator. The energy resolution is also improved by the selection of appropriate scintillation material. Accordingly we hope to reach the resolution of around $\sigma = 4\%$ for 1 MeV electrons, which corresponds to $\sigma = 2.2\%$ at $Q_{\beta\beta} \sim 3$ MeV.

An improvement of the resolution from 3 to 2.2% would result in the reduction of the $2\nu\beta\beta$ contribution by a factor of 6. This would improve the half-life limit by a factor of 2.5, and the mass limit by a substantial factor of 1.5. Here, the $2\nu\beta\beta$ contribution in the $0\nu\beta\beta$ window is evaluated by the spectrum shape analysis in the $0\nu\beta\beta$ peak region.

Thus, one may hope to obtain a half-life sensitivity of 6×10^{26} y, corresponding to the IH mass of around 32 meV $\pm$ 50% due to uncertainty in the $0\nu\beta\beta$ matrix element.

MOON-1 with $53 \times 53\,\mathrm{cm}^2$ plastic scintillators works well and can be expanded by a factor of 2 to the MOON scale ($\approx 100 \times 100\,\mathrm{cm}^2$) since the photon attenuation in the plate is less than a few percent.

Experimental studies of RI BG rejections with position-sensitive detector planes will be reported elsewhere. The MOON-type detector with the multilayer structure of scintillator plates can be universally used for $\beta\beta$ and other rare-decay experiments and for medical applications.

Acknowledgments

The authors thank Osaka University, OULNS, JASRI, MSCS, and NIRS for partial support in the present work. Two of the authors, H. Nakamura and H. Ejiri, are grateful to the former Oto mayor Mr. T. Kitamura and RCNP for supporting the Oto Cosmo Observatory and to Dr. H. Murayama for valuable discussions. The present work was partially supported by a Grant-in-Aid for Scientific Research (A) (No. 15204022) 2003–2006, from the Ministry of Education, Culture, Sports, Science and Technology.

1) H. Ejiri: J. Phys. Soc. Jpn. **74** (2005) 2101.
2) H. Ejiri: Phys. Rep. **338** (2000) 265.
3) J. Vergados: Phys. Rep. **361** (2002) 1.
4) S. Elliott and P. Vogel: Annu. Rev. Nucl. Part. Sci. **52** (2002) 115.
5) J. D. Suhonen and O. Civitarese: Phys. Rep. **300** (1998) 123.
6) F. Simkovic and A. Fassler: Prog. Part. Nucl. Phys. **48** (2002) 201.
7) H. Ejiri, J. Engel, R. Hazama, P. Krastev, N. Kudomi, and R. G. H. Robertson: Phys. Rev. Lett. **85** (2000) 2917.
8) H. Ejiri, K. Fushimi, T. Kamada, H. Kinoshita, H. Kobiki, H. Ohsumi, K. Okada, H. Sano, T. Shibata, T. Shima, N. Tanabe, J. Tanaka, T. Taniguchi, T. Watanabe, and N. Yamamoto: Phys. Lett. B **258** (1991) 17.
9) H. Ejiri, K. Higa, T. Kamada, H. Kobiki, K. Matsuoka, K. Okada, H. Sano, T. Shibata, T. Shima, N. Tanabe, J. Tanaka, T. Taniguchi, T. Watanabe, and N. Yamamoto: Nucl. Instrum. Methods Phys. Res., Sect. A **302** (1991) 304.
10) H. Ejiri, K. Fushimi, K. Hayashi, T. Kishimoto, N. Kudomi, K. Kume, H. Kuramoto, K. Matsuoka, H. Ohsumi, K. Takahisa, and S. Yoshida: Phys. Rev. C **63** (2001) 065501.
11) X. Sarazin: Proc. Neutrino Conf. 2004, Paris, 2004.
12) R. Arnold, C. Augier, J. Baker, A. Barabash, G. Broudin, V. Brudanin, A. J. Caffrey, E. Caurier, V. Egorov, K. Errahmane, A. I. Etienvre, J. L. Guyonnet, F. Hubert, Ph. Hubert, C. Jollet, S. Jullian, O. Kochetov, V. Kovalenko, S. Konovalov, D. Lalanne, F. Leccia, C. Longuemare, G. Lutter, Ch. Marquet, F. Mauger, F. Nowacki, H. Ohsumi, F. Piquemal, J. L. Reyss, R. Saakyan, X. Sarazin, L. Simard, F. Simkovic, Yu. Shitov, A. Smolnikov, I. Stekl, J. Suhonen, C. S. Sutton, G. Szklarz, J. Thomas, V. Timkin, V. Tretyak, V. Umatov, L. Vala, I. Vanushin, V. Vasilyev, V. Vorobel, and Ts. Vylov: Phys. Rev. Lett. **95** (2005) 182302.
13) C. E. Aalseth, D. Anderson, R. Arthur, F. T. Avignone III, C. Baktash, T. Ball, A. S. Barabash, R. L. Brodzinski, V. Brudanin, W. Bugg, A. E. Champagne, Y.-D. Chan, T. V. Cianciolo, J. I. Collar, R. W. Creswick, P. J. Doe, G. Dunham, S. Easterday, Yu. Efremenko, V. Egerov, H. Ejiri, S. R. Elliott, J. Ely, P. Fallon, H. A. Farach, R. J. Gaitskell, V. Gehman, R. Grzywacz, R. Hazma, H. Hime, T. Hossbach, D. Jordan, K. Kazkaz, J. D. Kephart, G. S. King III, O. Kochetov, S. Konovalov, R. T. Kouzes, K. T. Lesko, A. O. Macchiavelli, H. S. Miley, G. B. Mills, M. Nomachi, J. M. Palms, W. K. Pitts, A. W. P. Poon, D. C. Radford, J. H. Reeves, R. G. H. Robertson, R. M. Rohm, K. Rykaczewski, K. Saborov, Y. Sandukovsky, C. Shawley, V. Stekhanov, W. Tornow, R. G. van de Water, K. Vetter, R. A. Warner, J. Webb, J. F. Wilkerson, J. M. Wouters, A. R. Young, and V. Yumatov: Phys. Atom. Nucl. **67** (2004) 2002.
14) S. Scheonert: Proc. Neutrino 2006, Santa Fe, 2006.
15) C. Arnaboldi, F. T. Avignone III, J. Beeman, M. Barucci, M. Balata, C. Brofferio, C. Bucci, S. Cebrian, R. J. Creswick, S. Capelli, L.

Carbone, O. Cremonesi, A. de Ward, E. Fiorini, H. A. Farach, G. Frossati, A. Giuliani, D. Giugni, P. Gorla, E. E. Haller, I. G. Irastorza, R. J. McDonald, A. Morales, E. B. Norman, P. Negri, A. Nucciotti, M. Pedretti, C. Pobes, V. Palmieri, M. Pavan, G. Pessina, S. Pirro, E. Previtali, C. Rosenfeld, A. R. Smith, M. Sisti, G. Ventura, M. Vanzini, and L. Zanotti: Nucl. Instrum. Methods Phys. Res., Sect. A **518** (2004) 775.

16) R. Maruyama: Proc. Neutrino 2006, Santa Fe, 2006.
17) A. Pipke: Proc. Neutrino 2006, Santa Fe, 2006.
18) K. Zuber: Phys. Lett. B **519** (2001) 1.
19) T. Shima: Proc. APPEAL07 Workshop, CAST/JASRI, 2007.
20) P. Doe, H. Ejiri, S. R. Elliott, J. Engel, M. Finger, K. Fushimi, V. Gehman, A. Gorin, M. Greenfield, R. Hazama, K. Ichihara, T. Itahashi, P. Kavitov, V. Kekelidze, K. Kuroda, V. Kutsalo, K. Matsuoka, I. Manuilov, M. Nomachi, A. Para, A. Ryazantsev, R. G. H. Robertson, Y. Shichijo, L. C. Stonehill, T. Shima, G. Shirkov, A. Sisakian, Y. Sugaya, A. Titov, V. Vatulin, V. Voronov, O. E. Vilches, J. F. Wilkerson, D. I. Will, and S. Yoshida: Nucl. Phys. A **721** (2003) C517.
21) H. Ejiri, P. J. Doe, S. R. Elliott, J. Engel, M. Finger, J. A. Formaggio, K. Fushimi, V. Gehman, A. Gorin, M. Greenfield, R. Hazama, K. Ichihara, Y. Ikegami, H. Ishii, T. Itahashi, P. Kavitov, V. Kekelidze, K. Kuroda, V. Kutsalo, I. Manuilov, K. Matsuoka, H. Nakamura, M. Nomachi, T. Ogama, A. Para, A. Ryazantsev, R. G. H. Robertson, Y. Shichijo, T. Shima, Y. Shimada, G. Shirkov, A. Sisakian, L. C. Stonehill, Y. Sugaya, A. Titov, V. Vaturin, O. E. Vilches, V. Voronov, J. F. Wilkerson, D. I. Will, and S. Yoshida: Czech. J. Phys. **54** (2004) B317.
22) M. Nomachi, P. Doe, H. Ejiri, S. R. Elliott, J. Engel, M. Finger, J. A. Formaggio, K. Fushimi, V. Gehman, A. Gorin, M. Greenfield, R. Hazama, K. Ichihara, Y. Ikegami, H. Ishii, T. Itahashi, P. Kavitov, V. Kekelidze, K. Kuroda, V. Kutsalo, I. Manuilov, K. Matsuoka, H. Nakamura, T. Ogama, A. Para, K. Rielage, A. Ryazantsev, R. G. H. Robertson, Y. Shichijo, T. Shima, Y. Shimada, G. Shirkov, A. Sisakian, Y. Sugaya, A. Titov, V. Vatulin, O. E. Vilches, V. Voronov, J. F. Wilkerson, D. I. Will, and S. Yoshida: Nucl. Phys. B Proc. Suppl. **138** (2005) 221.
23) R. Hazama, P. Doe, H. Ejiri, S. R. Elliott, J. Engel, M. Finger, J. A. Formaggio, K. Fushimi, V. Gehman, A. Gorin, M. Greenfield, K. Ichihara, Y. Ikegami, H. Ishii, T. Itahashi, P. Kavitov, V. Kekelidze, K. Kuroda, V. Kutsalo, I. Manuilov, K. Matsuoka, H. Nakamura, M. Nomachi, A. Para, K. Rielage, A. Ryazantsev, R. G. H. Robertson, Y. Shichijo, T. Shima, Y. Shimada, G. Shirkov, A. Sisakian, Y. Sugaya, A. Titov, V. Vatulin, O. E. Vilches, V. Voronov, J. F. Wilkerson, D. I. Will, and S. Yoshida: Nucl. Phys. B Proc. Suppl. **138** (2005) 102.
24) H. Ejiri: Prog. Part. Nucl. Phys. **57** (2006) 153.
25) H. Ejiri: Mod. Phys. Lett. A **22** (2007) 1277.
26) H. Nakamura, H. Ejiri, K. Fushimi, K. Ichihara, K. Matsuoka, M. Nomachi, R. Hazama, S. Umehara, S. Yoshida, T. Ogama, T. Sakiuchi, V. H. Hai, and Y. Sugaya: J. Phys. Conf. Ser. **39** (2006) 350.
27) H. Nakamura: Dr. Thesis, Dissertation in Physics Graduate School of Science, Osaka University, Osaka, 2006.
28) R. Arnold, C. Augier, J. Baker, A. Barabash, G. Broudin, V. Brudanin, A. J. Caffrey, E. Caurier, V. Egorov, K. Errahmane, A. I. Etienvre, J. L. Guyonnet, F. Hubert, Ph. Hubert, C. Jollet, S. Jullian, O. Kochetov, V. Kovalenko, S. Konovalov, D. Lalanne, F. Leccia, C. Longuemare, G. Lutter, Ch. Marquet, F. Mauger, F. Nowacki, H. Ohsumi, F. Piquemal, J. L. Reyss, R. Saakyan, X. Sarazin, L. Simard, F. Simkovic, Yu. Shitov, A. Smolnikov, I. Stekl, J. Suhonen, C. S. Sutton, G. Szklarz, J. Thomas, V. Timkin, V. Tretyak, V. Umatov, L. Vala, I. Vanushin, V. Vasilyev, V. Vorobel, and Ts. Vylov: Phys. Rev. Lett. **95** (2005) 182302.
29) N. Kudomi, T. Shima, H. Ejiri, J. Tanaka, and T. Watanabe: Nucl. Instrum. Methods Phys. Res., Sect. A **322** (1992) 53.
30) RP408 specifications, REXON Components Inc., http://www.rexon.com/RP408.htm
31) R6236-01 specifications, Hamamatsu Corporation, http://sales.hamamatsu.com/assets/pdf/parts_R/R6236-01.pdf
32) CC/NET specifications, TOYO Corporation, http://www.toyo.co.jp/daq/ccnet/
33) SY527 specifications, Costruzioni Apparecchiature Elettroniche Nucleari spa, http://www.caen.it/nuclear/syproduct.php?mod=SY527
34) SY403 specifications, Costruzioni Apparecchiature Elettroniche Nucleari spa, http://www.caen.it/nuclear/syproduct.php?mod=SY403
35) H. Murayama, E. Tanaka, and N. Nohara: Nucl. Instrum. Methods **164** (1979) 447.
36) H. Nakamura, H. Ejiri, M. Nomachi, V. H. Hai, and H. Murayama: 2006 IEEE Nuclear Science Symp. Conf. Record, N30-144, 2006, p. 1170.